LAWRENCE
LIVERMORE
NATIONAL
LABORATORY

LLNL-JRNL-481058

Phosphate defects and apatite inclusions in coral skeletal aragonite revealed by solid-state NMR spectroscopy

H. E. Mason, P. Montagna, L. Kubista, M. Taviani, M. McCulloch, B. L. Phillips

April 22, 2011

Geochemica et Cosmochimica Acta

Disclaimer

Phosphate defects and apatite inclusions in coral skeletal aragonite revealed by solid-state NMR spectroscopy

Harris E. Mason[1†*], Paolo Montagna[2,3‡], Laura Kubista[1], Marco Taviani[3], Malcolm McCulloch[4§], Brian L. Phillips[1]

[1]Department of Geosciences, Stony Brook University, Stony Brook, New York 11794-2100
[2] Lamont-Doherty Earth Observatory Columbia University, 61 Route 9W, Palisades, NY 10964
[3]Istituto di Scienze Marine (ISMAR), Consiglio Nazionale delle Ricerche (CNR), Via P. Gobetti 101, 40122 Bologna, Italy
[4]Research School of Earth Sciences, Australian National University, Canberra, ACT 200, Australia
[*]corresponding author email: mason42@llnl.gov

[†]Present address: Physical Life Sciences Directorate, Lawrence Livermore National Laboratory, Livermore, CA 94550, USA.
[‡]Present address: Laboratoire des Sciences du Climat et l'Environnement, Gif-sur-Yvette, 91198, France
[§]Present address: University of Western Australia School of Earth and Environment Rm 138 M004 ARC Centre of Excellence in Coral Reef Studies
Crawley, Western Australia 6009

Abstract

Recent development of paleo-nutrient proxies based on the Phosphorus/Calcium (P/Ca) ratio in tropical- and deep-water corals (also known as cold-water corals) illustrate the necessity for understanding the processes by which P is incorporated into the coral skeletal aragonite. Here we apply single- and double-resonance solid-state nuclear magnetic resonance (NMR) spectroscopy to determine the speciation of P in coral aragonite. The results show that the majority of P occurs as phosphate defects in the aragonite structure, but in many samples a significant fraction of the P occurs also in crystalline hydroxylapatite inclusions. Quantification of the amount of hydroxylapatite indicates that its presence is not related simply to external environmental factors and that it can occur in varying abundance from different parts of the same corallite. Since there is currently no model available to describe the relationship between

dissolved inorganic phosphate and incorporation of apatite inclusions into carbonates, careful screening of samples which contain only phosphate in the aragonite structure or selective microsampling could improve proxy development.

Keywords: coral, phosphate, aragonite, NMR spectroscopy, apatite, ^{31}P, ^{1}H, ^{19}F

1. INTRODUCTION

It has been recently proposed that P/Ca ratios in the aragonite skeleton of corals record the concentration of ambient dissolved inorganic phosphorus (DIP), which, when combined with U-series chronology, could prove to be a useful paleo-nutrient proxy (Montagna et al. 2006; Anagnostou et al., 2007; LaVigne et al., 2008; LaVigne et al., 2010; Anagnostou et al., 2011). The amount of bioavailable phosphate in the photic zone of the surface ocean serves as a limit to primary productivity in some ocean basins. Since export of biomass to deep waters may act to drawdown atmospheric CO_2 (Broecker, 1982; Volk and Hoffert, 1985; Sarmiento et al., 1998), knowledge of past oceanic P concentrations is important to estimate the contribution of the "biological pump" to the levels of atmospheric CO_2. Montagna et al. (2006) noted that laser ablation inductively coupled plasma mass spectrometry (LA-ICPMS)-derived P/Ca ratios for aragonite septa from a variety of recent *Desmophyllum dianthus* coral samples were linearly related to the DIP concentration of the waters from which they were collected. This correlation was used to reconstruct paleo-nutrient data from a ~11 190 yr old sample. Unlike other trace elements used as paleo-environmental proxies, such as Ba, Sr and Cd, P cannot substitute simply into the aragonite crystal structure and its form in the coral aragonite is unknown (Dodge et al, 1984). The P speciation can be reasonably expected to influence the relationship between DIP concentration and aragonite P/Ca.

Geochemical models of trace element incorporation in calcite and aragonite typically rely on thermodynamic treatment of incorporation of the trace element into the mineral structure (Cohen and McConnaughey, 2003; Gagnon et al., 2007; Gaetani and Cohen, 2006). Phosphate co-precipitation, sorption, and desorption studies at phosphate solution concentrations less than 100 μM and near neutral pH suggest that inorganic phosphate incorporation in calcite can be

60 modeled by adsorption and subsequent incorporation of protonated phosphate groups (House and
61 Donaldson, 1986; Hinedi et al., 1992; Millero et al., 2001). It has also been shown in certain
62 cases that calcite with 60-100 μg/g P can contain crystalline Ca-phosphate inclusions that are
63 difficult to detect by microanalytical methods, suggesting that surface precipitates can form and
64 be subsequently encapsulated by continued crystal growth (Mason et al., 2007). Crystalline Ca-
65 phosphates can be difficult to nucleate and models that could account for the formation of such
66 P-rich precipitates via heterogeneous nucleation on calcium carbonate surfaces (Koutsoukos and
67 Nancollas, 1981) have yet to be fully explored. Therefore, to model the co-precipitation of
68 phosphate with calcium carbonate minerals it is desirable that phosphate is incorporated as a
69 structural constituent.
70 Solid-state ^{31}P nuclear magnetic resonance (NMR) spectroscopy is one potential
71 technique from which information on the distribution of P in coral aragonite might be obtained.
72 The ^{31}P NMR chemical shift is very sensitive to the bonding environment surrounding P and has
73 distinct, often characteristic values for crystalline phases. ^{31}P NMR techniques, primarily in the
74 liquid state, have been used extensively to determine P-speciation in soluble extracts from soil
75 samples and from marine sediments and particulate matter (for a review of these ^{31}P studies see
76 Cade-Menun, 2005, and Turner et al, 2005 for a review of extraction methods). Such methods
77 yield high resolution of organic P-species and are required for NMR investigation of materials
78 containing significant concentrations or paramagnetic ions (which cause severe linebroadening in
79 NMR spectra), but require harsh chemical treatments to separate various P fractions. In
80 addition, only a fraction of the P is extracted from the solids (typical recovery 30-60%), with
81 some P remaining in the insoluble residue (Ahlgren et al, 2007). Considering that coral
82 aragonite typically contains low concentrations of Fe and Mn, and bulk P concentrations just

83 within the NMR detection limit, it might be amenable to investigation by *in situ* solid-state ^{31}P
84 NMR methods.

85 Here we present a survey of solid-state ^{31}P NMR spectra of coral skeletal material that
86 illustrates the potential of the technique for determining the speciation of P in such materials, and
87 in other carbonate minerals as well. We use a variety of solid-state NMR spectroscopic methods
88 to characterize inorganic phosphate in a synthetic aragonite/phosphate coprecipitate and show
89 that the phosphate occurs within 3.2 Å of several carbonate groups, indicating that it is
90 incorporated in the aragonite structure. The similarity of these data with those obtained for coral
91 skeletal material provides strong evidence that structural phosphate defects are the principal P-
92 species in coral aragonite. Many coral samples also yield a ^{31}P NMR signal characteristic of
93 crystalline apatite that can represent a significant fraction of the bulk P, but the origin of which is
94 uncertain. These results support the use of P/Ca ratios for paleo-environmental proxies, but also
95 suggest that the proxy relationships might be improved by selecting samples lacking apatite
96 inclusions.
97

98 **2. EXPERIMENTAL METHODS**

99 **2.1. Sample Preparation**

100 *2.1.1. Coral Samples*

101 Subsamples of coral skeleton were selected from modern and subfossil corals lacking any
102 visible Fe-Mn-rich crust, checked under a binocular microscope and using thin sections under
103 plane and cross-polarized light. No major visible alterations (e.g. diagenetic alteration or
104 bioerosions) were evident. The P/Ca ratios and the P concentration for the coral samples were

obtained using LA-ICPMS following the procedures of Montagna et al (2006) and through solution ICPMS (see method below).

The sampling methods differed among the various coral species.

Desmophyllum dianthus and *Flabellum* sp.: fragments of the largest septum S1 were carefully removed by a diamond tipped saw attached to a dentist drill. Other subsamples were cut from the thecal wall and all the fragments of septa attached to the theca were mechanically abraded away using the same dentist drill. This allowed us to obtain samples representative of both the septum and the thecal margin. Two subsamples of *Desmophyllum dianthus* septa were crushed to pass a 250 μm analytical sieve and subjected to chemical cleaning; one was placed in a bleach solution (6% NaClO) and agitated for four days and another was treated using a method similar to those prescribed by Shen and Boyle (1988), Cheng et al (2000), and LaVigne et al. (2008) which are designed to remove sorbed metals and metal oxide coatings.

Lophelia pertusa: pieces of the thecal wall were obtained by cutting single corallites transversally. The part corresponding to the intersection between the wall and the septa (inside edge of the theca) was abraded and septa were completely removed.

Madrepora oculata: a piece of the coral was collected by cutting a corallite transversally. This coral portion contains both the thecal wall and the septa ("whole coral" reported in the text).

Porites sp.: a small rectangular parallelepiped was removed from a 7 mm slab previously obtained by cutting a coral core along the axis of growth. The subsample was taken at a distance of 12 cm from the top of the coral core in order to avoid the remnants of coral tissue.

128

129 *2.1.2 Synthetic aragonite/phosphate coprecipitates*

130 Aragonite/phosphate co-precipitation was undertaken using a seeded constant addition
131 method adapted from Zhong and Mucci (1993) and described by Reeder et al. (2000). The
132 aragonite seeds were synthesized by pumping separate solutions of 0.2 M $CaCl_2$ and 0.2 M
133 Na_2CO_3 using a dual syringe pump at a rate of 300 μl/min into a constantly stirring initial
134 solution containing 7 mM $CaCl_2$, 7 mM $NaHCO_3$, and 50 mM $MgCl_2$ which was being bubbled
135 with air. Each solution contained 0.1 M NaCl as background electrolyte. The aragonite seeds
136 were identified as pure aragonite by powder X-ray diffraction and analyzed by scanning electron
137 microscopy (SEM) to determine the average dimensions and morphology of the crystals,
138 revealing blocky crystals typically 3 μm wide by 4 to 10 μm long grouped into ball-shaped
139 clusters 40 to 50 μm in diameter. For phosphate co-precipitation, the same procedure was used
140 except 0.1 g of aragonite seed material was added to the initial growth solution, the
141 concentrations of reactants in the syringes were 0.1 M, and $NaHPO_4$ was added to the carbonate
142 syringe such that the phosphate concentration of the syringe ranged from 50 to 100 μM. A 0.1 M
143 $NaH^{13}CO_3$ solution replaced the Na_2CO_3 syringe to synthesize a ^{13}C-enriched sample. This
144 sample was prepared for $^{31}P/^{13}C$ double resonance NMR experiments where the low (1.1%)
145 natural abundance of the NMR active ^{13}C nucleus prevents observation of spectroscopic effects.
146 Periodically, solution was drawn from the growth solution to analyze total carbonate and reactive
147 phosphate concentrations, from which we determined that the phosphate concentration ranged
148 from 1 to 3 μM during crystal growth. After 4 to 5 h of reaction time the solid was collected,
149 filtered, and dried for 2 hrs in a 60° C oven. The P concentrations of the overgrowths were
150 calculated from the difference of phosphate added to the solution and that remaining in solution

151 at the end of the experiment (from measured reactive phosphate concentration and total solution
152 volume), estimating the mass of calcium carbonate precipitated from the amount of Ca added to
153 the growth solution. Powder X-ray diffraction indicates that all synthetic coprecipitates were
154 composed dominantly of aragonite, but that some contain as much as 9% calcite (Milliman and
155 Bornhold, 1973; Morse et al, 1985).
156
157 **2.2 Laser ablation ICPMS analysis**
158 The P/Ca ratios and the P concentrations were obtained following the analytical method
159 by Montagna et al. (2006, 2007). We used a high sensitivity pulsed laser ablation system,
160 coupled with a Fison PQII ICPMS with enhanced sensitivity. This laser ablation system housed
161 at RSES (Canberra) uses a LambdaPhysik LPX 120i argon fluoride 193nm excimer laser. All the
162 coral samples were scanned at 20 μm/s using a 20 μm wide and 220 μm long rectangular laser
163 beam mask with the laser pulsing at 5 Hz and an energy of 50 MJ. Before acquisition, surface
164 contamination was removed by pre-ablating the coral surfaces twice, with a 230 μm diameter
165 spot followed by the same rectangular slit used for the analysis. A pressed powder coral disc and
166 the NIST glass standard 612, chosen for its P concentration comparable to the coral samples,
167 were analysed before and after each run on the samples, together with the acquisition of the
168 background (gas blank) for 60s, allowing correction for long-term machine drift during analysis.
169 The precision for ^{31}P, calculated as the RSD (1σ/mean) of 60s acquisition on the NIST 612 was
170 ~ 6%.
171 The P concentrations of *Desmophyllum dianthus* and *Flabellum* sp were obtained both on
172 the outer faces of the S1 septum and on the thecal wall, whereas *Lophelia pertusa* was only

analysed along the theca. It was not possible for the *Porites* coral to discriminate between the theca and the septa and the P concentration represents an average over these skeletal portions.

2.3 Bulk solution ICPMS analysis

Analyses of ^{31}P and ^{43}Ca were determined by inductively coupled plasma mass spectrometry (ICP-MS) using the multi-collector Axiom in single collection mode at Lamont-Doherty Earth Observatory and following the standard addition method (Vandecasteele and Block, 1997) to correct for the matrix effect.

For some of the samples analysed by ^{31}P NMR, a precisely-weighted amount of coral powder was dissolved in double distilled HNO_3 and further diluted in 1% HNO_3 for the analysis by ICPMS. Procedural blank solutions were made with the same vials and acid used for the treatment of the samples. The analysis was carried out in two separate sessions: in the first session the concentration of P was measured in solutions with a final dilution factor of ~2000. The solutions were further diluted to a dilution factor of ~6000 and analysed for calcium concentration during a second analytical session.

A multi-element stock standard mixture was prepared gravimetrically with 1% HNO_3 and High-Purity Standards (Charleston, SC; 1000 ± 3μg mL^{-1} in 0.05% HNO_3 v/v for P; 1000 ± 3 μg mL^{-1} in 3% HNO_3 v/v for Mg and Sr; 10μg mL^{-1} in 4% HNO_3 for Ca), mixed in appropriate concentrations to match the typical composition of coral skeletons. Two four-point standard curves were prepared by adding increasing volumes of the stock solution to six pre-cleaned vials containing a constant volume of the unknown solutions (sample "G15606 S" and "DD Chile S-ct") and 1% HNO_3. The first point of each standard curve consists of one unspiked original sample. A third three-point standard curve was obtained by adding increasing amounts of a stock

196 solution containing solely P (High-Purity Standards) to pre-cleaned vials having a constant
197 volume of the unknown solution (sample "G16505 S") and 1% HNO_3. The results of the two
198 standardization methods were compared to verify the quality of the measurements.
199 A drift correction was performed by analysing an indium spiked mixed solution every five
200 samples and using a linear interpolation for all the elements. All the working solutions were also
201 spiked with indium as an internal standard to further correct for the instrumental drift. The
202 standards and unknown solutions were introduced to the plasma by a self-aspirating nebulizer
203 with an uptake rate of ~ 30 $\mu L\ min^{-1}$ in conjunction with a Cetac Aridus desolvating system.
204 Analytical reproducibility based on the RSD (1σ mean) of ten analyses of the Porites coral
205 standard JCp-1 (Geological Survey of Japan; run as an unknown) are ~ ±9.5% for P/Ca and P
206 concentration. Procedural blank for P, which was subtracted from the sample raw counts, was
207 typically < 20%.
208
209 **2.4. Solid-state NMR spectroscopy**
210 The ^{31}P single pulse magic angle spinning (SP/MAS) NMR and $^{31}P\{^{1}H\}$ cross
211 polarization (CP) MAS NMR spectra were collected on a 400 MHz Varian Inova spectrometer at
212 operating frequencies of 161.8 and 399.8 MHz for ^{31}P and ^{1}H, respectively. Samples were
213 contained in 7.5 mm outside diameter (o.d.) Si_3N_4 rotors and spun at 5 kHz. The probe and rotor
214 assemblies yielded no detectable ^{31}P NMR signal after several days of acquisition. However,
215 standard ZrO_2-based rotor sleeves can give a broad, weak ^{31}P signal in the orthophosphate region
216 (here taken to be the ^{31}P spectral region from -5 to 12 ppm; Turner et al, 1986). The ^{1}H SP/MAS
217 NMR and $^{1}H\{^{31}P\}$ rotational echo double resonance (REDOR) spectra were obtained using a
218 Chemagnetics probe assembly configured for 4 mm (o.d.) rotors and modified to yield very low

^{1}H background signal. The ^{31}P{^{1}H} Heteronuclear Correlation (HetCor) spectra were obtained using a probe configured for 3.2 mm (o.d.) rotors and were collected as a total of 100 hypercomplex points in *t1* with a 10 μs increment, corresponding to a 100 kHz spectral window in the ^{1}H dimension. A Carr-Purcell-Meiboom-Gill (CPMG) type acquisition was implemented to shorten the time needed to perform the HetCor experiment. The ^{19}F{^{31}P} REDOR, ^{31}P{^{13}C} SP/REDOR, and ^{1}H→ ^{31}P{^{13}C} CP/REDOR spectra were collected on a 500 MHz Varian Infinity Plus spectrometer at operating frequencies of 125.7, 202.3, 470.2, and 499.8 MHz for ^{13}C, ^{31}P, ^{19}F and ^{1}H respectively. The ^{19}F{^{31}P} REDOR spectra were collected using a Varian/Chemagnetics T3-type probe configured for 3.2 mm (o.d.) rotors and to give a very low ^{19}F background. The ^{31}P{^{13}C} SP and ^{1}H → ^{31}P{^{13}C} CP/REDOR spectra were collected using a Varian HXY probe configured for 4 mm (o.d) rotors. The ^{31}P MAS NMR spectra are referenced with respect to 85% phosphoric acid using hydroxylapatite as a secondary reference set to 2.65 ppm. The ^{1}H MAS NMR spectra are referenced with respect to tetramethylsilane using hydroxylapatite as a secondary reference set to 0.2 ppm. The ^{19}F spectra were referenced with respect to CCl_3F (C_6F_6 = 142 ppm).

3. RESULTS AND DISCUSSION

3.1. ^{31}P SP/MAS and ^{31}P{^{1}H} CP/MAS NMR

3.1.1 ^{31}P SP/MAS NMR of Coral Samples

We obtained solid-state ^{31}P NMR spectra for both aragonitic azooxanthellate and zooxanthellate coral samples having P contents ranging from 16 to 319 μg/g (Fig. 1; Table 1), including septa and thecal wall portions as well as whole coral samples. The ^{31}P{^{1}H} CP/MAS and ^{31}P SP/MAS spectra of a *Desmophyllum dianthus* septum (DD LM99-124) are presented in

Figure 2 and illustrate the typical spectral profile observed for most samples. These spectra can be described by a sum of two Gaussian peaks centered at ^{31}P chemical shifts (δ_P) of 2.7 and 4.0 ppm which have full-widths at half maximum (fwhm) of 1.7 and 6.4 ppm, respectively. Both peaks occur in the chemical shift range typical for orthophosphate species (Turner et al., 1986; Kolowith et al., 2001; Cade-Menun, 2005). Given the very low surface area of these samples and that the NMR signal arises from the entire sample volume, the peaks correspond mainly to P contained within the sample interior and cannot be attributed solely to surface adsorbed species. One possibility for the host of the P would be Fe-Mn oxide crust that may not have been removed from the surface abrasion techniques employed. However, any P occurring in Fe-Mn-oxides would not be observable under our experimental conditions, owing to extreme peak shifts and broadening of the ^{31}P resonance that would result from magnetic interactions with unpaired electrons (Grey et al., 2010). Therefore, we can rule out P associated with Fe-Mn oxides as the source of the observed ^{31}P NMR signal.

3.1.2. $^{31}P\{^1H\}$ CP/MAS NMR of Coral Samples

The two observed peaks exhibit distinct variation in $^{31}P\{^1H\}$ CP/MAS intensity with contact time (CP kinetics), which allows them to be separated easily depending on the acquisition conditions (Fig. 2). The CP kinetics in the simplest cases can be described by a sum of two exponential functions, in which intensity increases at short contact times with a time constant T_{PH} and then decreases at longer times with a time constant $T_{1\rho,H}$ (Kolodziejski and Klinowski, 2002). T_{PH} relates to the spatial proximity of P to H, and $T_{1\rho,H}$ to the relaxation of the ^1H nuclei, usually reflecting dynamical processes. The peak at $\delta_P = 2.7$ ppm (Fig. 2a) is dominant at long contact times due to a relaxation time of associated ^1H ($T_{1\rho,H} > 10$ ms) that is long compared to that for the peak at $\delta_P = 4.0$ ppm ($T_{1\rho,H} = 1$ ms). We assign this peak at $\delta_P =$

2.7 ppm to crystalline apatite, because its spectral characteristics closely match those reported previously for this phase, including its chemical shift, narrow width (characteristic of a highly ordered crystalline phase), and long $^{1}H \rightarrow {}^{31}P$ CP time (T_{PH} = 5 ms) and $T_{1\rho,H}$ (Rothwell et al., 1980; Belton et al., 1988; Kaflak et al., 2006). The broad peak at δ_P = 4.0 ppm dominates at short contact times (Fig. 2c) because of its much shorter $^{1}H \rightarrow {}^{31}P$ CP time (T_{PH} = 0.4 ms). This short T_{PH} value indicates that the P represented by the δ_P = 4.0 ppm peak are in close spatial proximity to rigid structural H (separations less than 4 Å). The two peaks fit to the CP/MAS spectra also describe the quantitative SP spectra, indicating that they represent the P distribution in the sample. With few exceptions, the spectra of the other deep-water corals are similar, differing only in the total signal intensity observed and relative proportion of that signal which is attributed to apatite. The chemically cleaned subsamples of *Desmophyllum dianthus* produce spectra which can be fit with peaks having the same chemical shifts and widths as those observed for the untreated samples. This result indicates that the P distribution in the cleaned samples is essentially similar to that in the same samples which had only undergone surface abrasion although the signal intensity is much reduced (Fig. 3).

3.1.3. Identification of additional minor P-species

Two other samples examined contain P environments not found in most of the other deep-water coral specimens. Spectra of a *Madrepora oculata* sample (MO CORAL2 75) contain a narrow peak at δ_P = -0.6 ppm (1.1 ppm fwhm), in addition to the broad peak near δ_P = 4 ppm common to all of the coral aragonite examined (Fig. 1g). The small width of the peak at -0.6 ppm suggests that it could arise from a crystalline inorganic phosphate phase (Rothwell et al., 1980; Belton et al., 1988; Mason et al., 2007), but the chemical shift is also consistent with phosphate esters (Cade-Menun, 2005) although such organic-P usually produces broader peaks

288 in solid-state ^{31}P NMR spectra. The origin of this peak was not investigated further, but its
289 presence illustrates that other P-containing materials could be present in coralline aragonite. The
290 *Porites* sp. (PO FR2004) sample we examined yields spectra containing a distinct peak at δ_P =
291 22.5 ppm (3.0 ppm fwhm), in addition to the broad peak near 4 ppm (Fig. 1h). This 22.5 ppm
292 chemical shift falls outside the range for phosphate, but is diagnostic of phosphonate (Glonek et
293 al., 1970; Kolowith et al., 2001, Cade-Menun, 2005), which contains C-P bonds and indicates the
294 presence of organic P in the sample. The *Madrepora* and *Porites* samples were not physically
295 cleaned, representing the whole coral skeleton and the sampled areas may include remnant
296 cellular material from either the coral polyp, products of bioerosion or endosymbionts (the latter
297 refers only to *Porites*), although phosphonates are known to adsorb strongly to calcite surfaces
298 (Sawada et al., 2003; Kan et al., 2005) and could interact similarly with aragonite and become
299 occluded during crystal growth. Since the NMR methods applied here cannot differentiate
300 between organic matter occluded in the aragonite, and that of remnant cellular material, we did
301 not explore these samples further.
302 *3.1.4. ^{31}P NMR of Synthetic Aragonite/phosphate coprecipitates*
303 A broad peak near δ_P = 4 ppm that is similar in both chemical shift, width, and CP
304 kinetics behavior to the broad peak observed for the coral samples dominates ^{31}P NMR spectra
305 of synthetic aragonite precipitated from solutions containing 1 - 3 μM DIP (Fig. 1 i-j). The
306 synthetic samples range in P concentration from 100 to 700 μg/g but their NMR spectra showed
307 no significant differences other than corresponding variations in signal intensity. The ^{31}P
308 CP/MAS spectra of these aragonite/phosphate coprecipitates also contain small, narrow peaks at
309 δ_P = 11.4 and 8.4 ppm that are not apparent in the quantitative ^{31}P SP/MAS spectra (Fig. 1 i,j),

suggesting they arise from phosphate associated with H in minor unidentified crystalline phases. A peak for apatite-like orthophosphate was not observed for any synthetic sample.

3.2. $^{31}P\{^{1}H\}$ HetCor NMR of Coral samples

Since the source of P in the synthetic samples is known we can assign the resulting NMR signal at δ_P = 4 ppm to inorganic phosphate. However, the source of the δ_P = 4 ppm peak in the coral samples cannot be inferred simply by comparison of the ^{31}P data because organic phosphate esters can give NMR peaks in the same ^{31}P chemical shift region (Teleman et al., 1999; Paytan et al., 2003; Cade-Menun, 2005). Distinction between organic and inorganic phosphate can be aided by ^{1}H NMR of the H associated with P, since the ^{1}H chemical shifts of organophosphate aliphatic H, which range from δ_H = 2.0 to 4.0 (Teleman et al., 1999), differ from those typical of HPO_4 groups and structural H_2O, in the 4.0 to 12.0 ppm range (Yesinowski and Eckert, 1987). We used $^{31}P\{^{1}H\}$ HetCor methods to selectively observe the ^{1}H spectra of only those H located near P, by detecting the ^{1}H from which magnetization is transferred during $^{1}H \rightarrow {}^{31}P$ CP. The ^{31}P-detected ^{1}H spectrum for a sample containing no apatite (DD G16505 S) shows a narrow peak at δ_H = 5.5 ppm that is underlain by a broad peak centered near 7.5 ppm (8.2 ppm fwhm) with a broad spinning sideband pattern (Fig. 4a). Neither peak occurs in the chemical shift range for aliphatic H in organophosphates (Teleman et al., 1999), but are consistent with assignment to molecular water undergoing restricted motion (5.5 ppm) and either rigid structural water or weakly H-bonded hydrogen phosphate (7.5 ppm). The synthetic aragonite/phosphate coprecipitate yielded a ^{31}P-detected ^{1}H spectrum (Fig. 4b) that is similar to that of the coral aragonite, containing a narrow peak at δ_H = 6 ppm and a broader peak centered near 8 ppm with a substantial spinning sideband pattern. Acquisition of these HetCor spectra required over one week of spectrometer time each, making it impractical to collect such data for

all of the coral samples. Considering that the broad peak near +4 ppm (the main signal in ^{31}P NMR spectra of the coral and synthetic samples) exhibits the same CP kinetics behavior in all samples and that the CP kinetics depends on the nature of H near P, it is reasonable to infer that the hydrogen environments observed in these HetCor spectra represent those associated with P in all samples which yield a similar ^{31}P NMR signal .

3.3. REDOR NMR

3.3.1. $^{31}P\{^{13}C\}$ REDOR NMR of synthetic aragonite/phosphate coprecipitates

The similarity of both the ^{31}P and (^{31}P-detected) ^{1}H NMR data for the coral aragonite to those for the synthetic aragonite/phosphate coprecipitate provides strong evidence that the nature of the phosphate is the same in both, i.e. orthophosphate. Based only on these NMR data, however, occurrence of phosphate as a substitution defect in the aragonite structure cannot be distinguished from a separate amorphous Ca-phosphate phase, since the latter yield similar spectra (Rothwell et al., 1980; Kaflak et al., 2006). A test for the presence of phosphate as defects in the aragonite structure can be obtained from a ^{31}P{^{13}C} REDOR NMR experiment, which depends on atomic-scale spatial proximity between ^{31}P and ^{13}C nuclei (within a few Å). For this experiment we used an aragonite/phosphate coprecipitate synthesized with ^{13}C-enriched carbonate because REDOR detects proximity to only the NMR-active ^{13}C isotope, the natural abundance of which (1.1%) is too low to yield a detectable REDOR effect for the very weak ^{31}P signal. The REDOR experiment compares two ^{31}P spectra, a control spectrum (S_0; Fig. 5a,c), containing signal from all P in the sample, and a REDOR spectrum (S; Fig. 5b,d) obtained in a similar manner as for S_0, except that dephasing pulses are applied at the ^{13}C frequency to re-introduce ^{31}P/^{13}C dipolar coupling, causing a decrease in signal intensity for P located near ^{13}C.

Simulations of the REDOR experiment indicate that no significant decrease in the ^{31}P peak intensity should occur for P located farther than 5 Å from ^{13}C.

The REDOR results at a 6.7 ms dephasing period show a large REDOR fraction $[(S_0\text{-}S)/S_0] = 0.7$ for the broad peak near $\delta_P = 4$ ppm. This value is similar to but somewhat lower than the maximum REDOR fraction (0.90) that could be expected for phosphate in the aragonite structure, estimated using the SPINEVOLUTION software (Veshort and Griffen, 2006) with a P/C configuration corresponding to substitution of phosphate for a carbonate group in the aragonite structure (6 C surrounding a central P at a distance of 3.2 Å; Fig. 6). A REDOR fraction smaller than this maximum value would be expected to result from structural disruption around a phosphate defect that would lead to fewer adjacent carbonate groups and/or longer P-C distances. However, multiple short (< 4 Å) P-C distances are required to explain this P/C REDOR result, which would seem possible only if the phosphate occurs in the structure of the carbonate phase. Similar REDOR results were obtained whether SP or CP excitation of ^{31}P was used (cf. Fig. 5a,b and c,d), strongly suggesting that much of the phosphate in aragonite is associated with H, and hence that H-bearing species play a role in accommodating the defect.

3.3.2. $^{1}H\{^{31}P\}$ and $^{19}F\{^{1}H\}$ REDOR NMR of coral samples

To determine the nature of the crystalline apatite inclusions that occur in some coral specimens, $^{1}H\{^{31}P\}$ and $^{19}F\{^{31}P\}$ REDOR NMR experiments were applied that would identify signals from H or F located in close proximity to P. Fluorapatite is a significant sink for phosphate in marine sediments (Kim et al., 1999) whereas biogenic apatite is composed primarily of carbonate-substituted hydroxylapatite (Elliot, 2002). The ^{19}F NMR spectrum for the *Flabellum* sp. theca sample (Fig. 7) is complex with multiple peaks. None of these peaks can be assigned to fluorapatite, which would occur at a chemical shift near -102 ppm (Braun and Jana,

1995), nor to any other phase for which ^{19}F NMR data have been reported in the literature. In addition, no $^{19}F\{^{31}P\}$ REDOR effect was observed for any ^{19}F peak, further indicating that no significant fraction of the F is associated with P, and hence that the apatite detected by ^{31}P NMR does not correspond to fluorapatite (Fig. 7). The $^{1}H\{^{31}P\}$ REDOR data (Fig. 8) were obtained for a *Desmophyllum dianthus* theca wall sample (DD CHILE Coral A). The control spectrum contains peaks at $\delta_H = 4.8$ and 1.5 ppm that do not exhibit decreased intensity in the REDOR spectrum, but which correspond well to signals assigned to water molecules and structural hydroxyl in a previous NMR study of calcium carbonate minerals (Gaffey, 1995). A very small peak occurs near $\delta_H = 0.2$ ppm that is near the chemical shift reported for hydroxylapatite (Yesinowski and Ekert, 1987), but which is marginally above the noise. This peak is clearly absent from the $^{1}H\{^{31}P\}$ REDOR spectrum (cf. Fig. 8a and b), indicating proximity to P and consistent with assignment to hydroxylapatite. These observations support the idea that the narrow peak in $^{31}P\{^{1}H\}$ CP spectra (Fig. 2a) arises from hydroxylapatite inclusions. Hydroxylapatite can also contain significant amounts of F; however, the hydroxyl peak in a mixed OH,F apatite would be expected to occur at a more positive chemical shift of about 1.2 to 1.4 ppm (Yesinowski and Ekert, 1987).

3.4. Quantification of the ^{31}P NMR signal

3.4.1. Relative hydroxylapatite content

Since acquisition of quantitative ^{31}P NMR spectra is extremely time-consuming, and impractical at P contents less than about 200 μg/g, we developed a relationship between relative intensities in ^{31}P SP/MAS and $^{31}P\{^{1}H\}$ CP/MAS spectra as a means to estimate the proportion of hydroxylapatite. Ideally the relative abundances of P corresponding to the peaks at $\delta_P = 2.7$ and 4 ppm would be derived through the careful integration of ^{31}P SP/MAS NMR spectra. However,

401 the low concentration of P in the samples and the long experimental relaxation delays (100's of
402 seconds) needed for quantitative results required almost 4 days of continuous spectrometer time
403 for some samples. Acquisition of a $^{31}P\{^{1}H\}$ CP/MAS NMR spectrum takes less than half the
404 time to obtain similar signal to noise ratio but the results are not quantitative without careful
405 analysis of CP kinetics (Kolodziejski and Klinowski, 2002), which can be time-consuming.
406 Therefore we estimated the relative abundance of apatite in the aragonitic coral skeletons from
407 CP/MAS spectra using a correlation between SP/MAS and CP/MAS intensities similar to that
408 described by Mason et al. (2007). The integrated intensity ratio of the peaks at 4 and 2.7 ppm
409 was determined from a SP spectrum acquired under quantitative conditions for a sample that
410 contained a high fraction of P in apatite (*Desmophyllum dianthus* septa sample: DD LM99 124).
411 These integrated intensities are proportional to the number of P in the respective environments,
412 meaning that 35±5% of the P in this sample occurs in apatite (peak at 2.7 ppm; Table 1). A
413 correction factor for CP/MAS spectra was then obtained by comparing this SP integrated
414 intensity ratio with that obtained from a CP/MAS spectrum of the same sample (1 ms contact
415 time). This correction factor was applied to the integrated intensity ratios obtained from
416 CP/MAS spectra of the other samples (1 ms contact time), yielding estimates for the percentage
417 of the ^{31}P-NMR detected P that occurs in apatite (Table 1, last column).

418 *3.4.2. P concentrations in the solid*

419 For several samples we independently measured P content using solution ICPMS in
420 addition to the LA-ICPMS analyses (Table 2). The solution ICPMS data provides an accurate
421 measure of the bulk P content of these samples and any disparity with the LA-ICPMS data was
422 attributed to the former method, which only analyzes the outer septal layers that may not
423 accurately reflect the bulk P content which is detected by NMR (Montagna et al., 2009;

Anagnostou et al., 2011). We also estimated the bulk P content for several samples from NMR data for comparison to the solution ICPMS results. The $^{31}P\{^{1}H\}$ CP/MAS NMR intensity of a sample of known bulk P content (synthetic aragonite containing 530 μg/g P as determined from the synthesis method) was compared to that for the unknown, collected under identical acquisition conditions (5 kHz spinning rate, 2 ms contact time, 2.0 s pulse delay) and scaled by mass and number of acquisitions. The synthetic aragonite yielded no detectable signal for apatite in CP/MAS spectra collected under conditions (10 ms contact time) that would favor its observation. We assume that the CP kinetics for the phosphate species are reasonably consistent among samples. Using this method we estimate 77 ±12 μg/g P for the DD-CHILE-TW, 200 ±28 μg/g P for the LP COBAS 109, and 126 ±18 μg/g P for the DD-CHILE-S samples. The concentrations for the two former samples agree well with the solution ICPMS analyses (Table 2). A portion of the sample DD-CHILE-TW that was chemically treated using the method designed to remove surface sorbed metals and metal oxides (DD-CHILE-TW-ct) showed a 54% reduction of P content to 35±5μg/g P. However, its ^{31}P CP/MAS NMR spectral profile did not differ significantly from that of the untreated material (cf. Fig 3). These results suggest that both the CP/MAS NMR spectra and the solution ICPMS methods are detecting the same pool of P, and that there is no significant fraction of P undetected by NMR. Furthermore, although the chemical cleaning procedure appears to preferentially remove aragonite around phosphate defects, there does not appear to be a significant difference in the bonding environment of the remaining phosphate.

3.4.3. Absolute hydroxylapatite content

Combining the relative abundance of hydroxylapatite derived from NMR with absolute P-contents from solution ICPMS data on the same sample, the amount of hydroxylapatite can be

447 estimated (Table 2). The result is a wide range of hydroxylapatite contents with no obvious
448 relationship to environmental factors such as depth and DIP. Nor do the concentrations of
449 hydroxylapatite correlate with the absolute P content determined from solution ICPMS. For
450 example, solution ICPMS data indicate DD G16505 TW contains only 22 μg/g P, but a large
451 percentage, 31%, occurs in hydroxylapatite. Moreover, there seems to be no clear correlation
452 between the apatite content and the preservation state of the corals (i.e. alive or fossil).

453 **3.5. Nature of P in coral aragonite**

454 Previous studies have suggested that the majority of P present in coral skeletons exists as
455 organic P-species (Dodge et al., 1984; Shotyk et al., 1995; LaVigne et al., 2008; Anagnostou et
456 al, 2011). This conclusion is based primarily on the results of various extraction procedures
457 relying on assumptions about the solubility and availability of organic versus inorganic P-
458 species. Since many studies assume that the acid-insoluble fraction contains only organic P, the
459 presence of relatively insoluble Ca-phosphates and possibly adsorption of phosphate onto
460 insoluble particles upon release by aragonite dissolution could skew the results of such an assay.
461 The results of the present study clearly show that the principal P-species present in most coral
462 aragonite samples closely resembles spectroscopically that produced by simply incorporating
463 dissolved inorganic phosphate during aragonite crystal growth.

464 The chemical cleaning methods employed here were originally designed to remove oxide
465 coatings and metals not incorporated into the aragonite structure. We do observe a substantial
466 decrease in the P concentration of the chemically treated samples. However, we attribute this
467 result to preferential dissolution of phosphate-rich regions, rather than the removal of P
468 associated with Fe-Mn or other metal oxide minerals. The NMR-derived P concentrations for
469 untreated samples are in reasonable agreement with those obtained by solution ICPMS methods

for the same samples. If a significant pool of P was associated with Fe-Mn crusts a large discrepancy between these values would be expected due to the inability of the NMR methods employed here to observe P associated with ions having unpaired electrons (Grey et al, 2010).

Montagna et al. (2009) and Anagnostou et al. (2011) have shown that the outer surface of coral septa produce higher LA-ICPMS derived P concentrations than the interior portions. Montagna et al. (2009) attributed these differences to the presence of P rich species such as hydroxylapatite in the outer septal surface. Since the NMR methods applied here are bulk techniques, we cannot differentiate between P contained in P rich outer layers and that contained within the less P rich internal microstructures. Given the results of Montagna et al. (2009), the observed drop in the NMR derived P concentrations after the application of the chemical cleaning methods could be attributed to the removal of defect and P rich portions of the coral aragonite which are more susceptible to dissolution.

3.6. Implications for further studies of P proxies in coral

A robust relationship between P/Ca ratio of coral aragonite and DIP suitable for use as a paleo-nutrient proxy would seem possible only if P occurs in the aragonite structure as phosphate defects. Simple trace element partitioning models developed for inorganic carbonates have been applied to surface and deep-water coral aragonite (Gaetani and Cohen, 2006; Sinclair and Risk, 2006; Gagnon et al., 2007), with the assumption that the coral polyp precipitates aragonite extracellularly from a calcifying fluid located between the polyp and the previous skeletal aragonite (Cohen and McConnaughey, 2003). This fluid consists of seawater, which is supersaturated respect to calcium carbonate through an enzymatic input of Ca^{2+} and removal of $2H^{+}$ (Cohen and McConnaughey, 2003). At least three processes could lead to P incorporation into coral aragonite, including encapsulation of surface precipitates, occlusion of organic matter,

493 and co-precipitation of dissolved inorganic phosphate as a substitution defect in the aragonite
494 likely initiated as a surface-adsorption complex. Of these, only in the latter could it be expected
495 that equilibrium is established between surface adsorbed phosphate and dissolved phosphate in
496 the aqueous phase as required for a linear partition coefficient (Rimstidt et al., 1998; Curti,
497 1999). Standard methodology used for proxy development such as LA-ICPMS, ion microprobe
498 and and x-ray adsorption spectroscopy (XAS) cannot yet provide the molecular-scale spatial
499 relationships between P and carbonate necessary to test whether P occurs in the aragonite
500 structure. The results obtained in the present study suggest that co-precipitation of phosphate is
501 the dominant process of P incorporation in deep-water corals lending support for the use of P/Ca
502 as a proxy. However, many of the studied samples also contain significant amounts of apatite
503 that could cause systematic error in proxy relationships, but which is easily detected using the
504 methods described here. Given the limited number of samples studied here, and the results
505 showing the incorporation of organo-P-species in some samples, screening of additional coral
506 samples may also be warranted. Taking into account possible contamination by crystalline
507 inclusions, careful selection of the coral portion to be analyzed (e.g. Montagna et al., 2009;
508 Anognastou et al., in press) should make it possible to obtain a more robust P/Ca vs. DIP
509 calibration, useful for paleo-nutrient reconstructions.
510
511 **Acknowledgments:**
512 This research was supported by the U.S. NSF (EAR-0819838), and instrumentation provided by
513 NSF CHE-03-21001. P. Montagna acknowledges financial support from the Marie Curie
514 International Outgoing Fellowship. Coral collection was funded by CNR grants, ESF
515 Moundforce and EU Hermes projects; Bruno Briano (Savona, Italy) and Günter Försterra kindly

516 supplied corals from offshore Madagascar and the Chilean fiords, respectively. Ship time of RV
517 Urania provided by CNR is gratefully acknowledged. This is ISMAR-Bologna scientific
518 contribution n. 1688. H.M. was supported through a U.S. Dept. of Education sponsored GAANN
519 fellowship (P200A060248).
520 This work performed under the auspices of the U.S. Department of Energy by Lawrence Livermore
521 National Laboratory under Contract DE-AC52-07NA27344.

522 **References**

523 Ahlgren J., Brabandere H. D., Reitzel K., Rydin E., Gogoll A., and Waldeback M. (2007)
524 Sediment phosphorus extractants for phosphorus-31 nuclear magnetic resonance
525 analyses: A quantitative evaluation. *J. Environ. Qual.* **36**, 892-898
526
527 Anagnostou E., Sherrell R. M., Adkins J. F., and Gagnon A. C. (2007) Phosphorus, barium and
528 boron in the deep-sea coral Desmophyllum dianthus: Preliminary calibrations. *Geochim.*
529 *Cosmochim. Acta* **71**, A22.
530
531 Anagnostou E., Sherrell R. M., Gagnon A., LaVigne M., Field M.P., McDonough W.F. (2011)
532 Seawater nutrient and carbonate ion concentrations recorded as P/Ca, Ba/Ca, and U/Ca in
533 the deep-sea coral Desmophyllum dianthus. *Geochim. Cosmochim. Acta* **75**, 2529-2543
534
535 Belton P. S., Harris R. K., and Wilkes P. J. (1988) Solid-state ^{31}P NMR studies of synthetic
536 inorganic calcium phosphates. *J. Phys. Chem. Solids* **49**, 21-27.
537
538 Braun M. and Jana C. (1995) ^{19}F NMR spectroscopy of fluoridated apatites. *Chem. Phys. Lett.*
539 **245**,19-22.
540
541 Broecker, W. S. (1982), Ocean geochemistry during glacial time, *Geochim. Cosmochim. Acta*,
542 **46**, 1689– 1705.
543
544 Cade-Menun B. J. (2005) Characterizing phosphorus in environmental and agricultural samples
545 by ^{31}P nuclear magnetic resonance spectroscopy. *Talanta* **66**, 359-371.
546
547 Cheng H., Adkins J., R. Edwards R.L., and Boyle E.A. (2000) U-Th dating of deep sea corals
548 *Geochim. Cosmochim. Acta* **64**, 2401-2416.
549
550 Cohen A. L. and McConnaughey T. A. (2003) Geochemical perspectives on coral
551 mineralization. *Rev. Min. Geochem.* **54**, 151-187.
552
553 Curti E. (1999) Coprecipitation of radionuclides with calcite: estimation of partition coefficients
554 based on a review of laboratory investigations and geochemical data. *Appl. Geochem.* **14,**
555 433-445.
556
557 Dodge R. E., Jickells T. D., Knap A. H., Boyd S., and Bak R. P. M. (1984) Reef-building coral
558 skeletons as chemical pollution (phosphorus) indicators. *Mar. Pollut. Bull.* **15**, 178-187.
559
560 Elliott J. C. (2002) Calcium phosphate biominerals. *Rev. Mineral. Geochem.* **48**, 427-453.
561
562 Gaetani G. A., and Cohen A. L. (2006) Element partitioning during precipitation of aragonite
563 from seawater: A framework for understanding paleoproxies. *Geochim. Cosmochim. Acta*
564 **70**, 4617-4634.
565
566 Gaffey S. J. (1995) H_2O and OH in echinoid calcite: A spectroscopic study. *Am. Mineral.* **80**,

947-959.

Gagnon A. C., Adkins J. F., Fernandez D. P., and Robinson L. F. (2007) Sr/Ca and Mg/Ca vital effects correlated with skeletal architecture in a scleractinian deep-sea coral and the role of Rayleigh fractionation. *Earth Planet. Sci. Lett.* **261**, 280-295.

Glonek T., Henderson T. O., Hilderbrand R. L., and Myers T. C. (1970) Biological phosphonates: determination by phosphorus-31 nuclear magnetic resonance. *Science* **169**, 192-194.

Grey, C. P.; Kim, J.; Middlemiss, D. S.; Chernova, N. A.; Zhu, B. Y. X.; Masquelier, C., Linking local environments and hyperfine shifts: a combined experimental and theoretical ^{31}P and ^{7}Li solid-state NMR study of paramagnetic Fe(III) phosphates. *J. Am. Chem. Soc.* **2010,** *132*, 16825-16840.

Hinedi Z. R., Goldberg S., Chang A. C., and Yesinowski J. P. (1992) A ^{31}P and ^{1}H MAS NMR study of phosphate sorption onto calcium carbonate. *J. Colloid Interf. Sci.* **152**, 141-160.

House W. A. and Donaldson L. (1986) Adsorption and coprecipitation of phosphate on calcite. *J. Colloid Interf. Sci.* **112**, 309-324.

LaVigne M., Field, M. P., Anagnostou, E., Grottoli, A. G., Wellington, G. M., and Sherrell, R. M. (2008) Skeletal P/Ca tracks upwelling in Gulf of Panama coral: Evidence for a new seawater phosphate proxy. *Geophys. Res. Lett.* **35**, L05604.

LaVigne M., Matthews K.A., Grottoli A.G., Cobb K.M, Anagnostou E., Cabioch G., and Sherrell R.M. (2010) Coral skeleton P/Ca proxy for seawater phosphate: Multi-colony calibration with a contemporaneous seawater phosphate record. *Geochim. Cosmochim. Acta* **74**, 1282-1293.

Kaflak A., Chmielewski D., Gorecki A., Slorarczyk A., and Kolodziejski W. (2006) Efficiency of ^{1}H→^{31}P cross-polarization in bone apatite and its mineral standards. *Solid State NMR* **29**, 345-348.

Kan A. T., Fu G. M., and Tomson M. B. (2005) Adsorption and precipitation of an aminoalkylphosphonate onto calcite. *J. Colloid Interf. Sci.* **281**, 275-284.

Kim D., Schuffert J. D., and Kastner M. (1999) Francolite authigenesis in California continental slope sediments and its implications for the marine P cycle. *Geochim. Cosmochim. Acta* **63**, 3477-3485.

Kolodziejski W. and Klinowski J. (2002) Kinetics of cross-polarization in solid-state NMR: A guide for chemists. *Chem. Rev.* **102**, 613-628.

Kolowith L. C., Ingall E. D., and Benner R. (2001) Composition and cycling of marine organic phosphorus. *Limnol. Oceanogr.* **46**, 309-320.

Koutsoukos P. G. and Nancollas G. H. (1981) Crystal growth of calcium phosphates: epitaxial considerations. *J. Cryst. Growth* **53**, 10-19.

Kumarsingh K., Laydoo R., Chen J. K., and Siung-Chang A. M. (1998) Historic records of phosphorus levels in the reef-building coral Montastrea annularis from Tobago, West Indies. *Mar. Pollut. Bull.* **36**, 1012-1018.

Mason H. E., Frisia S., Tang Y., Reeder R. J., and Phillips B. L. (2007) Phosphorus speciation in calcite speleothems determined from solid-state NMR spectroscopy. *Earth Planet. Sci. Lett.* **254**, 313-322.

Millero F., Huang F., Zhu X. R., Liu X. W., and Zhang J. Z. (2001) Adsorption and desorption of phosphate on calcite and aragonite in seawater. *Aquat. Geochem.* **7**, 33-56.

Milliman J. D. and Bornhold B. D., (1973) Peak height versus intensity analysis of X-ray diffraction data. *Sedimentology* **20**, 445-448

Montagna P., McCulloch M., Taviani M., Mazzoli C., and Vendrell B. (2006) Phosphorus in cold-water corals as a proxy for seawater nutrient chemistry. *Science* **312**, 1788-1791.

Montagna P., McCulloch M., Mazzoli C., Silenzi S. and Odorico R. (2007). The non-tropical coral Cladocora caespitosa as the new climate archive for the Mediterranean Sea: high-resolution (~ weekly) trace element systematics. Quaternary Science Review, 26, 441-462.

Montagna P., McCulloch M., Taviani M., Trotter J. and Silenzi S. (2009) An improved sampling method for P/Ca as a nutrient proxy. *Geochem. Cosmochim. Acta **73**, A895.*

Morse J. W., Zullig J. J., Bernstein L. D., Millero F. J., Milne P., Mucci A., and Choppin G. R. (1985) Chemistry of calcium carbonate-rich shallow water sediments in the Bahamas. *Am. J. Sci.* **285**, 147-185

Paytan A., Cade-Menun B. J., McLaughlin K., and Faul K. L. (2003) Selective phosphorus regeneration of sinking marine particles: evidence from ^{31}P-NMR. *Mar. Chem.* **82**, 55-70.

Reeder R. J., Nugent M., Lamble G. M., Tait C. D., and Morris D. E. (2000) Uranyl incorporation into calcite and aragonite: XAFS and luminescence studies. *Env. Sci. Technol.* **34**, 638-644.

Rimstidt J. D., Balog A., and Webb J. (1998) Distribution of trace elements between carbonate minerals and aqueous solutions. *Geochim. Cosmochim. Acta* **62**, 1851-1863.

Rothwell W. P., Waugh J. S., and Yesinowski J. P. (1980) High-resolution variable-temperature ^{31}P NMR of solid calcium phosphates. *J. Am. Chem. Soc.* **102**, 2637-2643.

659 Sarmiento J. L., Hughes T. M. C., Stouffer R. J., and Manabe S. (1998) Simulated response of
660 the ocean carbon cycle to anthropogenic climate warming, *Nature* **393**, 245–249.
661
662 Sawada K., Abdel-Aal N., Sekino H., and Satoh K. (2003) Adsorption of inorganic phosphates
663 and organic polyphosphonate on calcite. *J. Chem. Soc. Dalton Trans.* **3**, 342-347.
664
665 Sinclair D. J., and Risk M. J. (2006) A numerical model of trace-element coprecipitation in a
666 physicochemical calcification system: Application to coral biomineralization and trace-
667 element 'vital effects'. *Geochim. Cosmochim. Acta* **70**, 3855-3868.
668
669 Shen G.T. and Boyle E.A. (1988) Determination of lead, cadmium, and other trace metals in
670 annually-banded corals. *Chem. Geol.* **67**, 47-62.
671
672 Shotyk W., Immenhauserpotthast I., and Vogel H. A. (1995) Determination of Nitrate, Phosphate
673 and Organically Bound Phosphorus in Coral Skeletons by Ion Chromatography. *J.*
674 *Chromatogr. A.* **706**, 209-213.
675
676 Teleman A., Richard P., Toivari M., and Penttilla M. (1999) Identification and quantitation of
677 phosphorus metabolites in yeast neutral pH extracts by nuclear magnetic resonance
678 spectroscopy. *Anal. Biochem.* **272**, 71-79.
679
680 Turner G. L., Cade-Menun B. J., Condron L. M., and Newman S. (2005) Extraction of soil
681 organic phosphorus. *Talanta* **66**, 294-306
682
683 Turner B. L., Smith K. A., Kirkpatrick R. J., and Oldfield E. (1986) Structure and cation effects
684 on ^{31}P NMR chemical shifts and chemical-shift anisotropies of orthophosphates. *J. Magn.*
685 *Reson.* **70**, 408-415.
686
687 Vandecasteele C. and Block C.B. (1997). Modern methods for trace element determination. John
688 Wiley & Sons Ltd, West Sussex, England.
689
690 Veshtort M. and Griffin R. G. (2006) SPINEVOLUTION: A powerful tool for the simulation of
691 solid and liquid state NMR experiments. *J. Mag. Reson.* **178**, 248-282.
692
693 Volk T. and Hoffert M. I. (1985), Ocean carbon pumps: Analysis of relative strengths and
694 efficiencies in ocean-driven atmospheric CO_2, in The Carbon Cycle and Atmospheric
695 CO_2: Natural Variations Archean to Present, edited by E. T. Sundquist and W. S.
696 Broecker, pp. 99 – 110, AGU, Washington D. C.
697
698 Yesinowski J. P. and Eckert H. (1987) Hydrogen environments in calcium phosphates: ^{1}H MAS
699 NMR at high spinning speeds. *J. Am. Chem. Soc.* **109**, 6274-6282.
700
701 Zhong S. J. and Mucci A. (1993) Calcite precipitation in seawater using a constant addition
702 technique: A new overall reaction kinetic expression. *Geochim. Cosmochim. Acta* **57**,
703 1409-1417.

Table 1: Coral samples studied by ^{31}P NMR, including the location, depth, and dissolved inorganic phosphorus (DIP) concentration of waters in which sample grew at the time of collection. Percentage of the total P contained in apatite (% P_{Ap}) was estimated by NMR (See text). All corals were live at the time of collection unless otherwise indicated (f = fossil). The LA-ICPMS precision (RSD) for the phosphorus concentration is ~ 6% (see methods).

Name	Species	Portion	location	depth (m)	DIP (μM)	[P] in solid (μg/g)	%P_{Ap}
DD LM99-124	*Desmophyllum dianthus* (fossil)	Septa	Tyrrhenian Sea	377-411	-	119±60	35±5
DD CHILE CoralA	*Desmophyllum dianthus*	Theca	Chilean Fjords	30	1.78±0.36	No Data	41±7
DD G16505 S	*Desmophyllum dianthus*	Septa	Western Pacific	406	1.26±0.18	202±55	0
DD G16505 TW	*Desmophyllum dianthus*	Theca	Western Pacific	406	1.26±0.18	17±5	31±5
F MAD S	*Flabellum* sp.	Septa	Madagascar	800-1000	1.99-2.35	87±21	0
F MAD TW	*Flabellum* sp.	Theca	Madagascar	800-1000	1.99-2.35	55±11	34±5
DD CHILE S	*Desmophyllum dianthus*	Septa	Chilean Fjords	30	1.78±0.36	319±79	8.3±9
DD CHILE TW	*Desmophyllum dianthus*	Theca	Chilean Fjords	30	1.78±0.36	35±7.6	0
LP CORAL2 75	*Lophelia pertusa*	Theca	Ionian Sea	828-818	0.26±0.01	32±12	15±3
LP COBAS 109	*Lophelia pertusa* (fossil)	Theca	Baleares Islands	366	-	106±19	0
MO CORAL2 75	*Madrepora oculata*	Whole coral	Ionian Sea	828-818	0.26±0.01	No Data	0
PO FR2004	*Porites* sp.	Whole coral	Fitsroy Reef (Great Barrier Reef)	5	0.12-0.15	36±11	0

Table 2: P concentration data for select coral samples obtained from solution ICPMS and NMR methods. $[P]_{Ap}$ determined from % P_{Ap} values in Table 1. The solution ICPMS precision (RSD) for the P/Ca and P concentration is ~ 9.5% (see methods).

Name	**P/Ca (µmol/mol)**	**[P] ICPMS (µg/g)**	**[P] NMR (µg/g)**	**$[P]_{Ap\ NMR/ICPMS}$ (µg/g)**
DD G16505 S	121±11	38±4	No Data	0
DD G16505 TW	68±6	22±2	No Data	7±1
DD CHILE TW	No Data	No Data	77±12	No Data
DD CHILE TW-ct	No Data	No Data	35±5	No Data
DD CHILE S	331±31	118±11	126±18	10±1
DD CHILE S-ct	253±24	83±8	No Data	No Data
LP CORAL2 75	49±5	16±2	No Data	2±1
LP COBAS 109	374±36	123±12	200±28	0

Figure Captions:

Figure 1: ^{31}P NMR spectra for coral aragonite and aragonite/phosphate coprecipitate samples. **a-f)** ^{31}P{^{1}H} CP/MAS NMR spectra of coral septa and thecal wall aragonite **a)** septa and **b)** thecal wall of *Desmophyllum dianthus* (DD CHILE TW) **c)** septa and **d)** thecal wall of *Flabellum sp.* (F MAD TW) **e)** live collected (LP CORAL2 75) and **f)** fossil (LP COBAS 109) samples of *Lophelia pertusa* thecal wall **g-h)** ^{31}P{^{1}H} CP/MAS spectra of whole coral samples *Madrepora oculata* (MO CORAL2 75) and *Porites sp.* (PO FR2004), respectively. **i-j)** ^{31}P{^{1}H} CP/MAS spectra of aragonite/phosphate co-precipitated samples containing **i)** 306 μg/g and **j)** 102 μg/g P. All spectra obtained using a spinning rate of 5 kHz, 2 ms CP contact time, and 2 s pulse delay except **h)** 10 kHz spinning rate and 120 s pulse delay and **i-j)** 2 ms CP contact time, 2 s pulse delay and a spinning rate of 3 kHz. Asterisks mark the location of spinning sidebands.

Figure 2: ^{31}P MAS NMR spectra collected of *Desmophyllum dianthus* coral septa (DD LM99 124) from the Tyrrhenian Sea. **a-c)** ^{31}P{^{1}H} CP/MAS NMR spectra collected at a 3 kHz spinning rate and 2 s pulse delay for 4672 acquisitions using contact times of **a)** 10 ms, **b)** 1 ms, and **c)** 0.2 ms. **d)** ^{31}P SP/MAS NMR spectrum obtained with a 5 kHz spinning rate and 120 s pulse delay for 819 acquisitions. **e)** Components of the least squares fit to the spectrum shown in **d),** vertically offset for clarity.

Figure 3: ^{31}P{^{1}H} CP/MAS NMR spectra of septa for *Desmophyllum dianthus* sample DD CHILE S collected using 2 s pulse delay and 5 ms CP contact time at a spinning rate of 3 kHz. **a)** Spectra taken from a sample that was only physically cleaned to remove surface contaminants.

b) Spectra taken from a sample that underwent the chemical treatment outlined by LaVigne et. al. (2008). Asterisks mark the location of spinning sidebands.

Figure 4: ^{31}P-detected ^{1}H MAS/NMR obtained from summed projections of 2-d ^{31}P{^{1}H} CPMG HetCor data for **a)** *Desmophyllum dianthus* coral sample DD G16505 S and **b)** synthetic aragonite/phosphate coprecipitate (520 μg/g P) . Both were collected at 2 ms contact time and 10 kHz spinning rate. Asterisks mark the location of spinning sidebands.

Figure 5: ^{31}P{^{13}C} REDOR NMR spectral sets for ^{13}C-enriched aragonite/phosphate coprecipitate collected at a 6 kHz spinning rate and 6.7 ms dephasing period. **SP:** Standard SP/REDOR, **CP:** CP/REDOR with 2 ms ^{31}P{^{1}H} CP preparation. **a, d)** Echo control spectra (S_0) **b, c)** ^{31}P{^{13}C} REDOR spectra (S). Diamonds denote background signal from rotor and asterisks mark the location of spinning sidebands. S_0, S pairs are plotted at the same absolute intensity.

Figure 6: Simulated ^{31}P{^{13}C} REDOR dephasing curve for a ^{31}P surrounded by 6 ^{13}C at a distance of 3.2 Å. Dashed line occurs at the dephasing period where experimental data is reported.

Figure 7: ^{19}F{^{31}P} REDOR NMR spectra collected for the *Flabellum* sp. theca sample (F MAD S) collected at a spinning rate of 25 kHz, a 100 s pulse delay, and 1.28 ms dephasing period for 1488 acquisitions. **Top**: ^{19}F Spin-echo control spectrum (S_0) **Bottom**: ^{19}F{^{31}P} REDOR spectrum (S). Asterisks mark the location of spinning sidebands.

Figure 8: $^{1}H\{^{31}P\}$ REDOR NMR spectra for a *Desmophyllum dianthus* (DD CHILE CoralA) sample collected at a spinning rate of 15 kHz, pulse delay of 2 s, and dephasing period of 4.4 ms for 62 928 aquisitions. Spectra are shown at 5 times vertical exaggeration and truncated. **a)** $^{1}H\{^{31}P\}$ Spin-echo control spectrum (S_0) **b)** $^{1}H\{^{31}P\}$ REDOR spectrum (S). Dotted line denotes the chemical shift of hydroxylapatite (0.2 ppm) in the Spin-echo control spectrum. Inset: Expanded view of the Spin-echo control spectra over the range of 4 to -2 ppm.

766 **Figure 1:**

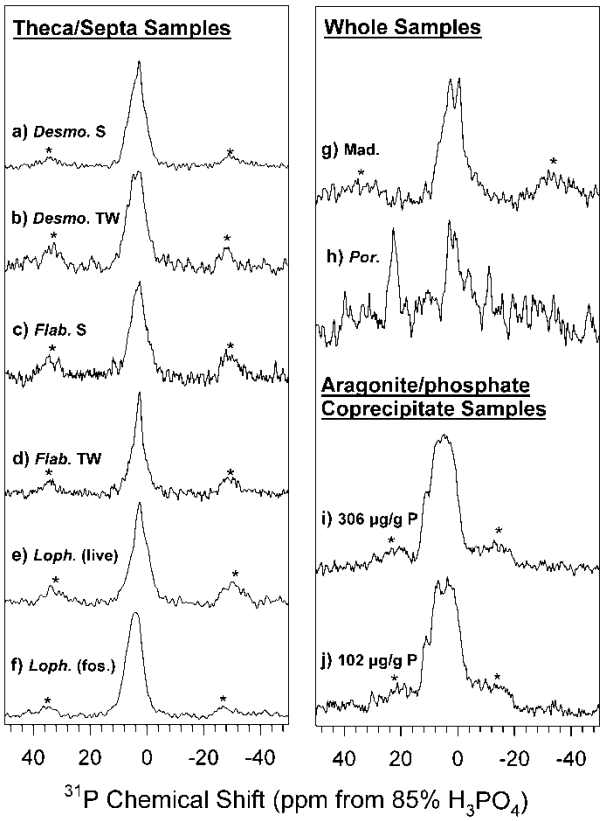

767
768

769 **Figure 2:**

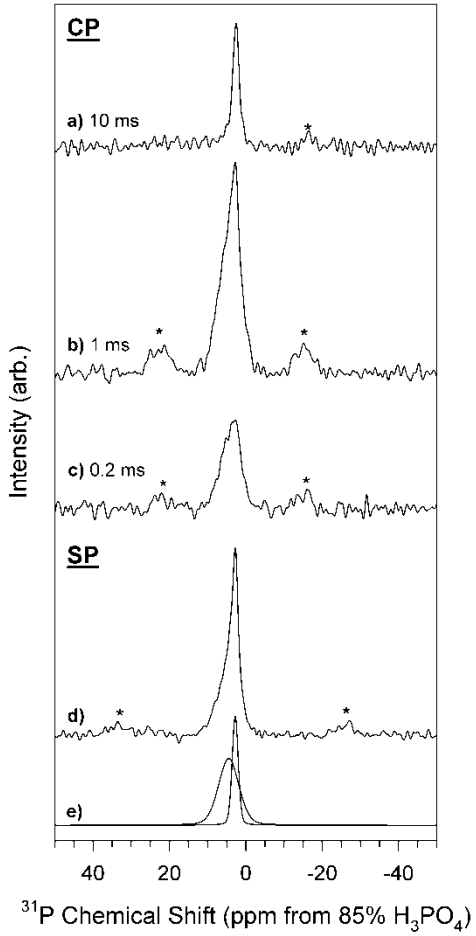

770
771
772
773

774 **Figure 3:**

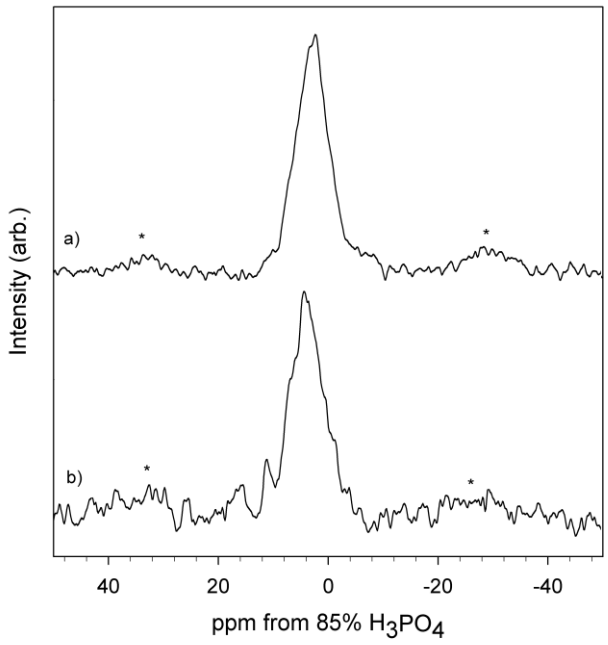

775
776

777 **Figure 4:**

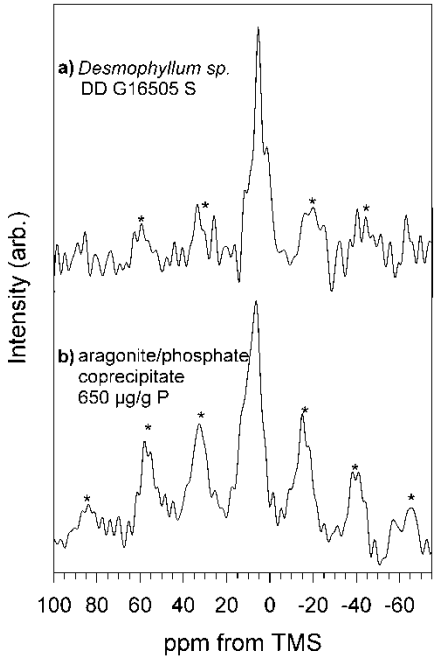

778
779
780

781 **Figure 5:**

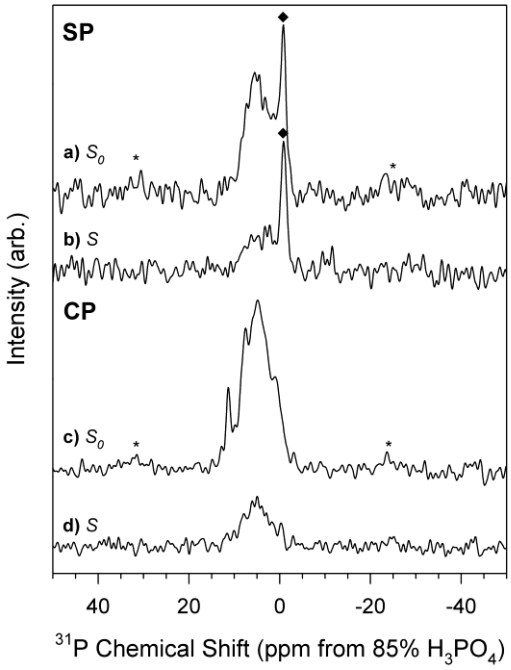

782
783

784 **Figure 6:**

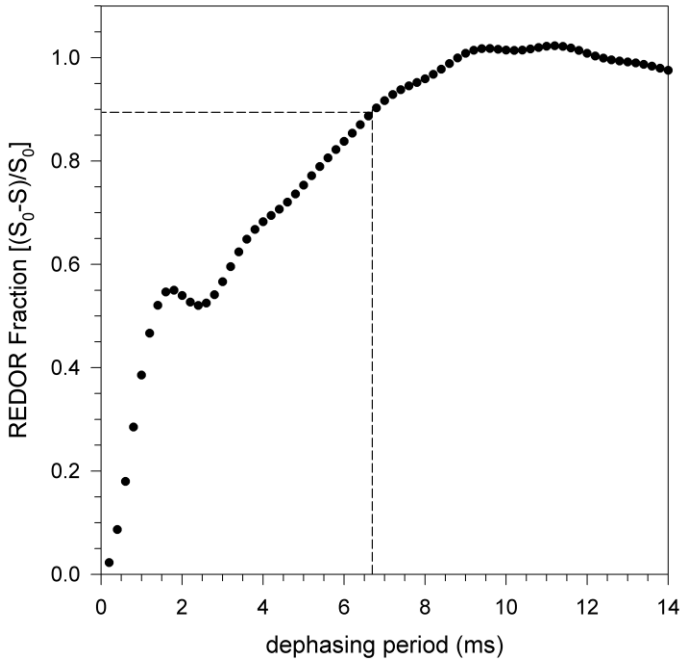

785
786
787

788 **Figure 7:**

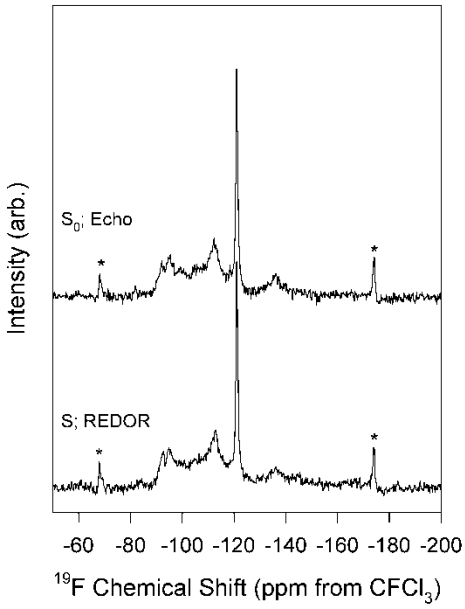

789
790

791 **Figure 8:**

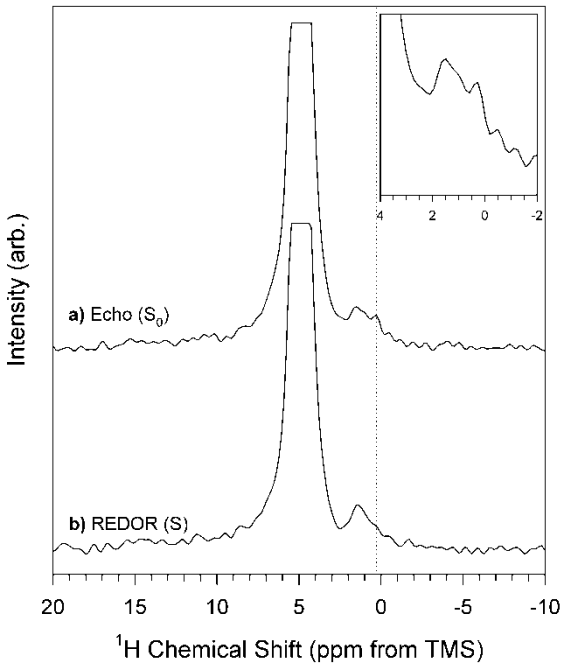

792